American Mineralogist, Volume 100, pages 2371–2379, 2015

Roebling Medal Lecture

Trace element partitioning into sulfide: How lithophile elements become chalcophile and vice versa† 🔓

Bernard J. Wood[1,*] and Ekaterina S. Kiseeva[1]

[1]Department of Earth Sciences, University of Oxford, South Parks Road, Oxford OX1 3AN, U.K.

Abstract

Sulfides, although modally of low abundance in most igneous rocks, have strong influences on the geochemical behavior of many elements including Pb, Cu, Ni, and the PGEs. In a recent paper, we demonstrated a simple relationship between the sulfide-silicate partition coefficients $D_M^{\text{sulf/sil}}$ of such elements and the FeO content of the coexisting silicate melt (Kiseeva and Wood 2013).

$$\log D_M^{\text{sulf/sil}} \approx \text{A} - \frac{n}{2}\log\left[\text{FeO}\right]$$

where n is the valency of element M, [FeO] is the concentration of FeO in the silicate in wt%, and A is a constant that depends on temperature and pressure. Elements that closely obey the simple model are Pb, In, Sb, Cd, Co, Zn, and Cr. We show here, however, that the fitted slope n depends not only on the valency of element M, but also on how M interacts with oxygen, the dissolution of which as FeO in the sulfide increases as the FeO content of the silicate melt increases.

To take account of interactions of trace element M with FeO dissolved in the sulfide we introduce an additional parameter $\varepsilon_{MS_{n/2}}^{FeO_{sulf}}$ (Wagner 1962), which represents the difference between the lithophile and chalcophile properties of M and those of Fe. If $\varepsilon_{MS_{n/2}}^{FeO_{sulf}}$ is positive, then element M is more chalcophile than Fe and if negative more lithophile.

We performed experiments to investigate partitioning of lithophile Nb, Ta, Ce, and Ti between sulfide and simplified basaltic melt and find that they all exhibit, as expected, concave upward behavior on a plot of log$D$ vs. log[FeO]. New experiments on Cu at low FeO contents confirm that it is more chalcophile than Fe, yielding a concave-downward curve of log$D$ vs. log[FeO]. The combined results mean that nominally lithophile elements may partition more strongly into sulfide than nominally chalcophile elements at either very low or very high FeO contents of the silicate melt. For example, as the FeO content of the silicate melt declines below about 1 wt%, the partition coefficient of Cu, $D_{Cu}^{\text{sulf/sil}}$ declines to an unusually low value ($D_{Cu}^{\text{sulf/sil}}$ ~80), whereas those for Nb ($D_{Nb}^{\text{sulf/sil}}$ ~600), and rare earths (REE's) increase strongly. Under these conditions, Nb is, therefore, substantially more "chalcophile" than Cu in that it partitions much more strongly into sulfide.

The implications of these observations for the Earth are that under a wide range of conditions one would expect significant partitioning of REE, Nb, Ta, Ti, and other lithophile elements into sulfides. Wohlers and Wood (2015) have, for example, shown that the partitioning of U and the REE into sulfides at low FeO content of the silicate is sufficiently pronounced that addition of a reduced sulfur-rich body to the accreting Earth could generate observable fractionation of Nd from Sm and, together with S, transfer sufficient U to the core to provide a significant energy source for the geodynamo.

Keywords: Sulfides, chalcophile elements, partitioning behavior, trace elements, lithophile elements

Introduction

Although the concentration of sulfur in the silicate Earth is only about 250 ppm (McDonough and Sun 1995), sulfur and sulfides are major geochemical agents. Their impacts extend from immiscible droplets in basaltic melts, which control the concentrations of chalcophile elements such as Pb and Cu in differentiating magmas, through high-temperature hydrothermal deposits and low-temperature lead-zinc deposits. In the case of Pb, for example, the Ce/Pb and Nd/Pb ratios of N-MORB appear to be essentially constant at ~25 and ~20, respectively (Hart and Gaetani 2006; Hofmann et al. 1986). Since Pb is much more incompatible than Ce and Nd in mantle silicate minerals (Hart and Gaetani 2006), it seems that partitioning of Pb into volumetrically very small amounts of sulfide exerts the principal control on behavior of this element in partial melting and igneous differentiation. Similar arguments have

* E-mail: berniew@earth.ox.ac.uk

† 🔓 Open access: Article available to all readers online.

been made in favor of sulfide precipitation exerting the major control on the behavior of Cu (Lee et al. 2012) during generation and evolution of island arc basalts. Lee et al. (2012) found that Cu is strongly incompatible in most silicate phases and that with $D_{Cu}^{sulf/sil}$ in the range 600–1200 the small amounts of sulfide present in the sub-arc mantle should control the Cu contents of magmas. Furthermore, they suggest that the low Cu concentrations in primitive arc basalts imply oxygen fugacities of ~FMQ (similar to MORB) and that some differentiated magmas reached about FMQ+1.3 log units before precipitating sulfide (Lee et al. 2012). Many other chalcophile elements (Cd, In for example) are economically important, which makes the interpretation and understanding of their geochemical behavior of considerable value.

In addition to economic importance, sulfide and chalcophile elements have frequently been proposed to have played important roles in the accretion and differentiation of the Earth. The strong depletion of S in the silicate Earth, relative to elements of similar volatility such as Zn is likely due to its strong partitioning into the core during accretion (Dreibus and Palme 1996). This may have been in the form of a late-added sulfide matte (O'Neill 1991; Wood and Halliday 2005). Both Wood and Halliday (2005) and Hart and Gaetani (2006) argue that partitioning of Pb into mantle sulfide and extraction of such sulfide to the core could be responsible for the "lead paradox," the observation that silicate Earth lies to the right of the "geochron" on a $^{207}Pb/^{204}Pb$ vs. $^{206}Pb/^{204}Pb$ diagram.

Theoretical development

Given the importance of sulfides in controlling the geochemical behavior of many elements, we recently attempted to systematize trace element partitioning between sulfide melt and silicate liquid (Kiseeva and Wood 2013). We started with the simplest equilibrium describing partitioning of a chalcophile element, Ni, for example between the two liquid phases. This can be written as follows:

$$\underset{\text{silicate}}{NiO} + 0.5S_2 = \underset{\text{sulfide}}{NiS} + 0.5O_2 \quad (1)$$

In that case, at fixed pressure and temperature the equilibrium constant is defined as:

$$K_1 = \frac{a_{NiS}^{sulf}}{a_{NiO}^{sil}} \cdot \frac{f_{O_2}^{0.5}}{f_{S_2}^{0.5}} \quad (2)$$

where K_1 is the equilibrium constant and a_i and f_i are activity and fugacity of i, respectively. Generally speaking, sulfide liquids in the Earth are FeS-rich so neither the activity of NiO (in silicate) nor that of NiS (in sulfide) is close to 1. To a good approximation, however, we can usually replace activity ratios by concentration ratios, which leads to:

$$\frac{a_{NiS}^{sulf}}{a_{NiO}^{sil}} \approx \frac{[Ni]^{sulf}}{[Ni]^{sil}} = D_M^{sulf/sil} = K_1' \cdot \frac{f_{S_2}^{0.5}}{f_{O_2}^{0.5}} \quad (3)$$

where K_1' is a modified equilibrium constant in terms of concentration. Thus, the partition coefficients D_i must depend on the ratio of sulfur fugacity to oxygen fugacity. At one atmosphere pressure, oxygen and sulfur fugacities are fairly readily controlled using CO_2-CO-SO_2 mixtures, which enable K_1' to be determined as a function of temperature. Many chalcophile elements are volatile, however, which means that experiments are most easily performed at high pressure. In that case, it is much more difficult to control sulfur fugacity and oxygen fugacity control requires the presence of a free fluid phase. However, as shown by Kiseeva and Wood (2013), we can dispense with sulfur and oxygen fugacity control if we consider partitioning of the elements of interest in terms of an exchange reaction with the major element Fe:

$$\underset{\text{silicate}}{NiO} + \underset{\text{sulfide}}{FeS} = \underset{\text{silicate}}{FeO} + \underset{\text{sulfide}}{NiS} \quad (4)$$

At saturation of the silicate melt with sulfide the Ni partition coefficient $D_{Ni}^{sulf/sil}$ can be expressed by a modified equilibrium constant K_2' and the activities of iron species, which are much easier to measure and control than the fugacities of the gaseous species:

$$D_M^{sulf/sil} = K_4' \cdot \frac{a_{FeS}^{sulf}}{a_{FeO}^{sil}} \quad (5)$$

If we use a pure FeS liquid with trace Ni, then the activity of FeS is essentially 1.0, so we can take logarithms and rearrange Equation 5 to:

$$\log D_{Ni}^{sulf/sil} = \log K_4' - \log a_{FeO}^{sil} \quad (6)$$

More generally, where the trace element of interest M has a different valency from Fe and the activity of FeO in the silicate is a linear function of its concentration, Equation 6 may be expressed as:

$$\log D_M^{sulf/sil} \approx A - \frac{n}{2}\log[FeO] \quad (7)$$

In Equation 7, A and n depend on the equilibrium constant for the exchange reaction and valency, respectively, and [FeO] is the FeO concentration in the silicate in appropriate units. Kiseeva and Wood (2013) showed that, at fixed temperature and pressure, Equation 7 describes the sulfide-silicate partitioning behavior of several elements (notably Pb, In, Sb, Cd, Co, Zn, Cr) extremely well. These elements all show linear dependences of $\log D_i$ on log[FeO] if the sulfide is pure FeS. In nature, however, the major cations in magmatic sulfide liquids are generally mixtures of Fe with Ni and Cu. Kiseeva and Wood (2013) also found that, to a good approximation, one could assume ideal Fe-Ni-Cu solution so that the activity of FeS is reduced from 1.0 by the cation fraction of Fe in the sulfide. We incorporated this correction in the FeO term as follows:

$$[FeO]_{corrected} = \frac{[FeO]_{silicate}}{[Fe/(Fe+Ni+Cu)]_{sulfide}} \quad (8)$$

Despite simple and predictable partitioning behavior for many elements, several important elements (Ni, Cu, Ag, Mn, Tl) show strongly non-linear dependences of $\log D_i$ on log[FeO] and we were unable to assign them to any one particular category in terms of affinity for sulfide. It is the purpose of this paper to expand on the ideas of Kiseeva and Wood (2013) and to test our

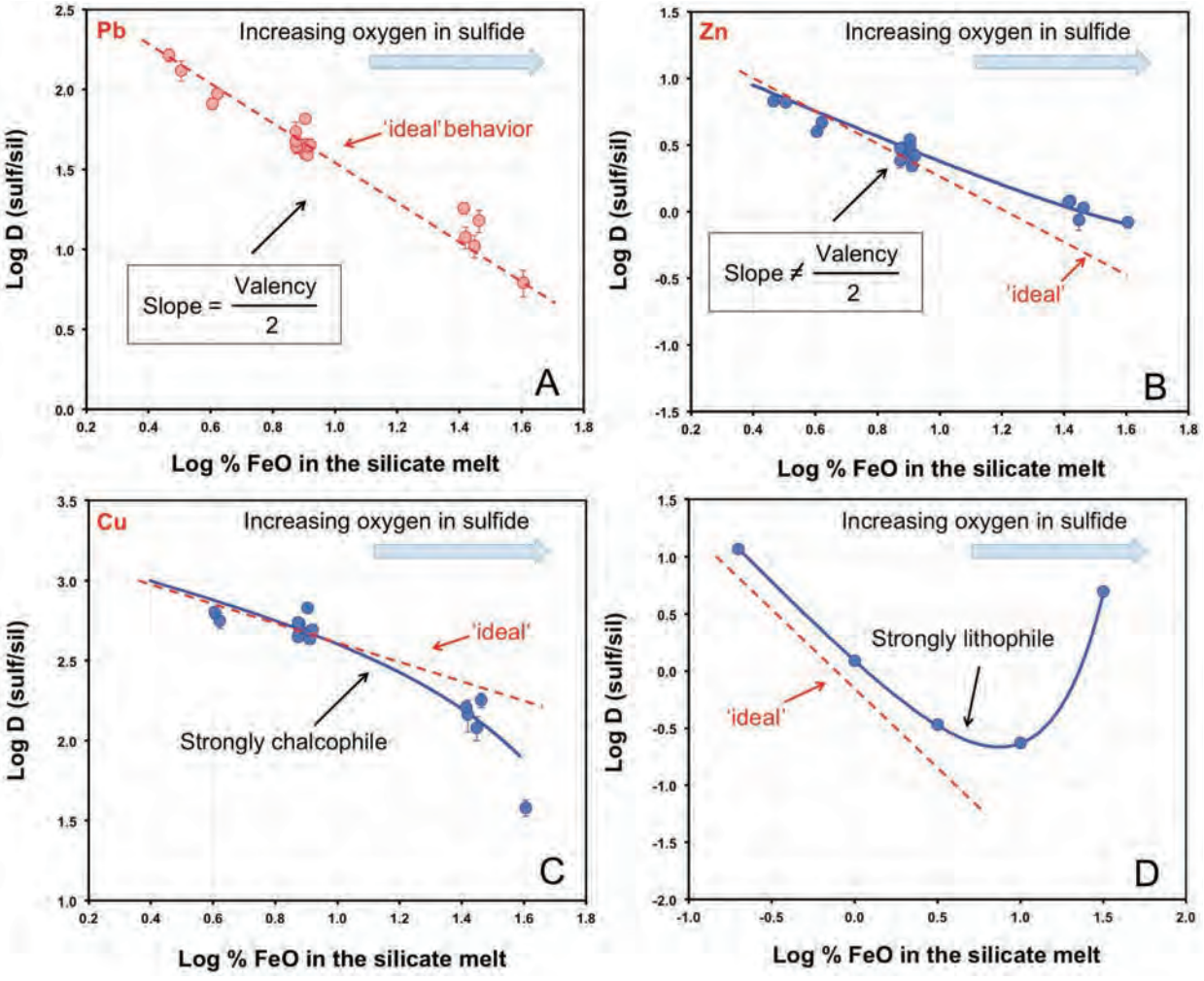

Figure 1. This figure shows sulfide-silicate partitioning behavior for trace elements as predicted from Equations 7 and 12. (**a**) Partition coefficients $D_{Pb}^{sulf/sil}$ at 1.5 GPa/1400 °C measured by Kiseeva and Wood (2013, 2015) as a function of the FeO content of the silicate melt (wt%). Dashed line of "ideal" behavior refers to theoretical slope of valency/2. (**b**) Partitioning of Zn from the same authors showing flatter than "ideal" slope due to interactions of Zn with oxygen in sulfide. (**c**) Partitioning of Cu from the same authors showing steeper than "ideal" slope due to interactions with oxygen, given by a positive value of $\varepsilon_{CuS_{0.5}}^{FeO_{sulf}}$ from Equation 12. (**d**) Theoretical plot of logD vs. log[FeO] for a strongly lithophile element with negative $\varepsilon_{MS_{n/2}}^{FeO_{sulf}}$ from Equation 12.

ideas on the potential roles of oxygen in the sulfide and of sulfur in the silicate on controlling partitioning of many elements.

Oxygen and sulfur in sulfides and their influences on partitioning

As observed by Kiseeva and Wood (2013), there is an excellent correlation between the FeO content of the silicate melt and the oxygen content of the coexisting sulfide. At 1.5 GPa and 1400 °C this corresponds to:

$$O(sulf) \cong 0.24FeO(sil) \quad (9)$$

where O and FeO are both in wt%. (Note that with more data the slope has been updated from the original 0.23.) At 10 wt% FeO in the silicate, therefore, the O content of the sulfide is 2.4 wt% approximately, which corresponds to an O/(S+O) of about 0.13 in sulfide. Thus, at 10% FeO in the silicate, 13% of the anions in the sulfide are oxygen rather than sulfur and the FeO content of the sulfide is about the same as that in the silicate:

$$[FeO](sulf) \approx [FeO](sil) \quad (10)$$

We hypothesized that this significant replacement of S by O would affect partitioning of both chalcophile and *lithophile* elements into sulfide.

Figure 1 shows idealized and "non-ideal" partitioning behavior based on Equation 7. Ideal behavior (Fig. 1a) yields, of course, a straight line of slope $n/2$ where n is the valency of the trace ion. We show in Figure 1a that Pb closely approximates "ideal" partitioning behavior. Figure 1b shows the situation when the trace ion is slightly more lithophile than Fe. A linear correlation

is observed but the slope is less negative if the element, like Zn, is more lithophile than Fe. Similar behavior is exhibited by Ga, V, and Ge. If the element is more chalcophile than Fe (e.g., Co), the slope is more negative than the "ideal" slope. Figure 1c shows the expected partitioning behavior for elements that are much more chalcophile than Fe and that exhibit downward curvature on the plot of logD_i vs. log[FeO]. The example shown is Cu, but Ni and Ag behave similarly. Strongly lithophile elements should show *upward* curvature on a plot of logD_i vs. log[FeO] (Fig. 1d), but since partitioning of lithophile elements into sulfide is not generally regarded as important, this behavior has not previously been explored. One of our purposes here is to show that some important lithophile elements do partition into sulfides in the manner depicted in Figure 1d. A second purpose is to investigate partitioning of both chalcophile and lithophile elements into sulfide at very low FeO content of the silicate. As will be shown, the results are surprising and would have been very difficult to predict. We continue with a description of partitioning experiments aimed at studying the lithophile elements Ti, Ce, Nb, and Ta together with additional results on chalcophile Cu.

Experimental and analytical procedures

Experimental methods

Starting materials consisted of mixtures of ~50% FeS and ~50% synthetic silicate, by weight. The silicate constituent was a composition close to the 1.5 GPa eutectic composition in the system anorthite–diopside–forsterite ($An_{50}Di_{28}Fo_{22}$) (Presnall et al. 1978) (Table 1). The end-members anorthite, diopside, and forsterite were pre-synthesized from mixtures of analytical-grade SiO_2, Al_2O_3, and MgO, combined with $CaCO_3$. The oxide mixes were decarbonated at 950 °C for 2 h, pelletized, and fired twice for 5 h at 1150 °C with grinding and re-pelletizing in between each firing. Iron oxide (as $Fe_{0.95}O$) was added after firing in some experiments to increase FeO activity. In other cases $FeSi_2$ was added to consume the oxide layer that forms on powdered FeS (in the bottle) and to drive the FeO content of the silicate to as low a value as possible. Occasionally this leads to precipitation of a second immiscible Fe-Si liquid in addition to the sulfide. Fortunately in such cases the two liquids are physically separate from one another. Small amounts of Ni (as NiS ≤1%) and/or Cu (as oxide) were sometimes added to the sulfide starting mixture to provide a second internal standard for laser ablation-inductively coupled plasma-mass spectrometry (LA-ICP-MS) analysis of the metallic phase. Ti, Nb, and Ta were added as 1–2% oxides to the silicate mix. Ce was present as a contaminant. The starting materials were ground under acetone before being dried prior to the experiment.

Starting mixtures were loaded into 3 mm O.D., 1 mm I.D. graphite capsules and experiments performed in an end-loaded piston-cylinder apparatus. The experimental assembly consisted of a 12.7 mm O.D. calcium fluoride cylinder with inner graphite heater of 8 mm O.D. and 6 mm I.D. At temperatures above 1450 °C the outer sleeve was replaced by an outer thin-walled barium carbonate sleeve and inner silica glass sleeve. Internal (to the heater) spacers were of 6 mm O.D. machineable MgO. The capsule was surrounded and separated from the graphite furnace by a 6 mm O.D. ring of machineable MgO. The experimental pressure was based on the calibration of McDade et al. (2002).

Temperature was controlled and measured using a C-type ($W_{95}Re_5$–$W_{74}Re_{26}$) thermocouple separated from the capsule by a 0.5 mm alumina disk. Based on our previous work (Kiseeva and Wood 2013) experiment durations of 30 min are sufficient to approach equilibrium at 1400 °C. All experiments were therefore performed for 30 min or longer. After quenching, products were mounted in acrylic resin, individually sectioned and hand-polished using water-based lubricants and diamond pastes. During the experiment the sulfide segregates into large blobs, several hundred micrometers across, while the silicate glass also generally exhibits large sulfide-free areas (Fig. 2). This good physical separation enables analysis of both phases using the methods described below.

The experimental products were analyzed using a JEOL JXA8600 electron microprobe at the Department of Archaeology at the University of Oxford. WDS analyses were conducted using a 15 kV accelerating voltage and 20 to 100 nA beam current with a defocused 10 µm spot to improve averaging of both silicate and sulfide phases. At least 25 repeat analyses were collected for the silicate and sulfide parts of each charge. Counting times were as follows: 30 s peak and 15 s background for major elements (e.g., Si, Al, Ca, Mg); 60–120 s peak and 30–60 s background for minor elements (Ti, Cu, Ni, Nb, Ta). The peak count time for Fe was adjusted from 30–60 s on peak (half of this time on background) depending on anticipated concentration. A range of synthetic and natural standards was used for calibration. Standards for sulfide analysis were galena (S); Nb, Ta, Ni, and Cu metals, rutile (Ti); and hematite (Fe, O). Standards for silicate glass analysis were wollastonite (Ca, Si), periclase (Mg), rutile (Ti), albite (Na, Al), fowlerite (Mn), orthoclase (K), and hematite (Fe). Natural almandine was used as a secondary standard for the silicate phases. Oxygen in the sulfide was determined using the *K*α peak and a LDE pseudocrystal as described by Kiseeva and Wood (2013). Results are given in Tables 2 and 3.

Trace-element concentrations of the coexisting silicate glasses and sulfides were determined on experimental products using LA-ICP-MS. Measurements were made using a Perkin Elmer Nexion quadrupole mass spectrometer coupled to a New Wave Research UP213 Nd: YAG laser at the University of Oxford. Beam diameters of 50 µm were used for both silicate and sulfide phases. The following

Table 1. Experimental conditions

Run no.	Starting composition	Duration (h)	Trace elements	*T* (°C)
390	CMAS+FeS	1	TR2	1400
395	CMAS+FeS	1	TR2	1400
1321	MORB+FeS+NiS(tr)	2	TR2	1400
1322	MORB+FeS+NiS(tr)	2	TR2	1400
1323	(MORB+30%FeO)+FeS+NiS(tr)	2	TR2	1400
1324	(MORB+20%FeO)+FeS+NiS(tr)	2	TR2	1400
1325	(MORB+40%FeO)+FeS+NiS(tr)	2	TR2	1400
1412	CMAS+FeS+10%$FeSi_2$	1	TR2	1420
1418	CMAS+FeS+3%$FeSi_2$	0.5	TR	1460
1419	CMAS+FeS	0.5	TR	1460
1425	CMAS+FeS+4%NiS+15%$FeSi_2$	0.5	TR	1460
KK38-1	CMAS+FeS+30%$FeSi_2$	1.5	TR	1400

Notes: All experiments performed in graphite capsules. NiS(tr) = less than 0.5% added in the bulk started mixture. MORB = taken from Falloon and Green (1987) (column 2). CMAS = $Fo_{22}Di_{28}An_{50}$. TR contains Cu, In, Tl, Pb, Ag, Zn, Cr, V, Co, Sb, and Cd as oxides with Cu_2O double that of other oxides. TR2 contains Nb and Ta.

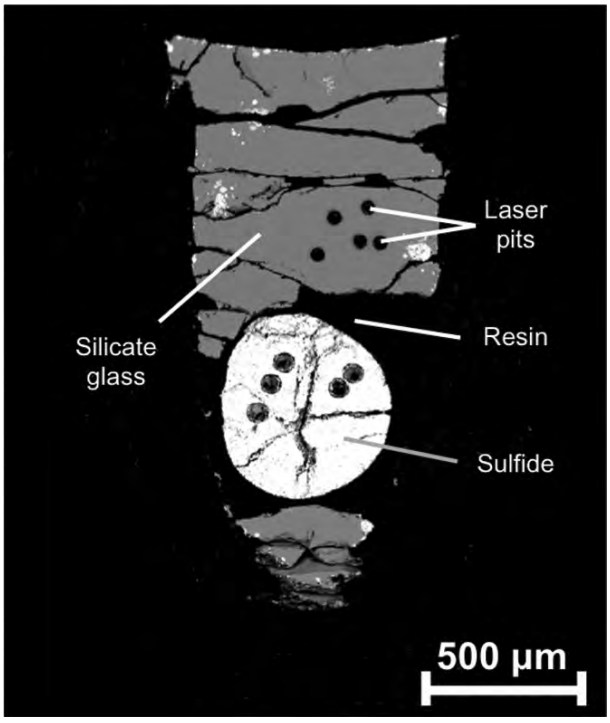

Figure 2. Backscattered electron image of products of experiment 1323. Slight "speckling" of sulfide surface is due to polishing imperfections.

masses were counted: ^{24}Mg, ^{27}Al, ^{29}Si, ^{44}Ca,^{47}Ti, ^{57}Fe, ^{60}Ni, ^{65}Cu, ^{93}Nb, ^{140}Ce, ^{181}Ta with yields calibrated on NIST 610 glass standard as the primary standard, NIST 612 glass and USGS glass standard BCR-2G being used as secondary standards to monitor the accuracy of the calibration. The NIST 610 calibration was routinely checked after every 8–12 unknowns and results corrected for calibration drift. Internal standards for the silicate and sulfide glasses were principally the Si and Fe contents, respectively, which had been measured by electron microprobe. The LA-ICP-MS analyses (Table 4) involved determining background counts for the first 20 s of each 60 s analysis and then collecting counts for each mass during the 40 s period of ablation. Background counts were minimized by including a 60–90 s "wash-out" between each collection. Raw counts were collected on the ICP-MS in peak-hopping mode and displayed in time-resolved format. Data reduction used the GLITTER software package (http://www.glitter-gemoc.com/). This allowed each ablation to be monitored to identify heterogeneities such as small sulfide inclusions in the silicate and compositional variations with depth. Silicate analyses obviously contaminated by sulfide inclusions were rare and were discarded.

Because the Fe content of NIST 610 is only 460 ppm and backgrounds are high we required additional internal cross-checks for the sulfide analyses. Therefore either Ti and/or Ni or Cu contents of the sulfides were measured by both electron microprobe and LA-ICP-MS. As can be seen in Table 4 and in agreement with the observations of Kiseeva and Wood (2013) the concordance between microprobe and LA-ICP-MS results for these elements is generally very good, which gives us confidence in the partition coefficients determined by LA-ICP-MS (Table 5).

TABLE 3. Major element compositions of the sulfide (wt%)

Exp. no.	*n*	O	S	Fe	Ni	Cu	Ti	Totals
390	41	1.14	36.89	62.88	b.d.l.	b.d.l.	n.m.	100.91
	σ	0.30	0.38	0.40	–	–	n.m.	
395	33	1.23	35.93	62.29	b.d.l.	0.14	n.m.	99.60
	σ	0.24	0.50	0.62	–	0.06	n.m.	
1321	15	1.49	36.44	62.65	n.m.	n.m.	0.0077	100.59
	σ	0.58	0.85	0.84	n.m.	n.m.	0.0044	
1322	42	3.08	33.61	64.37	n.m.	n.m.	0.0135	101.08
	σ	0.36	0.48	0.60	n.m.	n.m.	0.0050	
1323	44	5.55	30.60	65.04	n.m.	n.m.	0.0254	101.22
	σ	0.41	0.51	0.55	n.m.	n.m.	0.0063	
1324	38	4.03	32.45	64.67	n.m.	n.m.	0.0225	101.18
	σ	0.75	0.93	0.58	n.m.	n.m.	0.0066	
1325	63	7.19	28.62	64.86	b.d.l.	n.m.	0.0434	100.71
	σ	0.41	0.53	0.41	–	n.m.	0.0072	
1412	15	0.81	30.99	63.96	0.39	0.11	0.3013	96.56
	σ	0.27	0.80	0.98	0.05	0.04	0.0564	
1418	15	1.03	36.13	59.27	n.m.	0.28	n.m.	96.71
	σ	0.30	0.37	0.43	n.m.	0.04	n.m.	
1419	15	1.00	35.83	60.33	n.m.	0.16	n.m.	97.32
	σ	0.26	0.49	0.51	n.m.	0.02	n.m.	
1425	63	1.21	30.55	67.09	0.03	n.m.	n.m.	98.88
	σ	0.38	2.66	2.44	0.02	n.m.	n.m.	
KK38-1	28	0.17	32.57	60.78	1.58	0.86	n.m.	95.97
	σ	0.33	1.47	1.69	0.52	0.17	n.m.	

Notes: Besides listed results, sulfides contain trace elements Cu, Pb, Zn, Cd, Ga, Ge, Ag, Sb, Mn, Co, In, Tl, Cr in the following total amounts: 1412 (0.92 wt%), 1418 (1.3 wt%), 1419 (0.8 wt%), 1425 (2.05 wt%), KK38-1 (4.6 wt%).

LITHOPHILE ELEMENT PARTITIONING INTO SULFIDE

Although lithophile elements are not conventionally considered of interest in sulfide behavior, Figure 1d suggests that, at high and low FeO contents of the silicate melt, there should be significant partitioning of many lithophile elements into the sulfide phase. Figure 3 shows partitioning results for Ce, Ti, Nb, and Ta at 1.5 GPa and temperatures of 1400–1460 °C. As can be seen, all three elements show the predicted behavior for lithophile elements sketched in Figure 1d, which suggests a U-shaped dependence of logD_M on log[FeO]. These elements follow oxygen and partition more strongly into sulfide as FeO contents of sulfide and silicate increase. At low FeO contents, the low activity of FeO in the silicate forces $D_M^{\text{sulf/sil}}$ to increase in the manner predicted from Equation 7 with a negative slope of 0.5 times the valency. In principle, then, the concave-upward behavior implies that lithophile elements such as these may partition strongly into sulfide and become "chalcophile" under conditions of either very low or very high FeO content. We discuss this is more detail below.

The dependence of $D_M^{\text{sulf/sil}}$ for these lithophile elements on the oxygen content of sulfide may be parameterized using the ε-model of non-ideal interactions in metallic liquids (Ma 2001; Wagner 1962). For the case of highly dilute trace element *M* this model yields, for $MS_{n/2}$ dissolved in, as shown by Kiseeva and Wood (2013), an approximately ideal FeS-FeO matrix:

TABLE 2. Major element compositions of the silicate glass (wt%)

Exp. no.	*n*	SiO_2	TiO_2	Al_2O_3	FeO	MnO	MgO	CaO	Na_2O	K_2O	Nb_2O_5	Ta_2O_5	S	Totals
390	29	42.74	0.88	16.54	4.07	b.d.l.	15.94	16.08	b.d.l.	b.d.l.	0.92	1.02	0.59	98.77
	σ	0.79	0.03	0.32	0.13	–	0.23	0.29	–	–	0.06	0.09	0.06	
395	34	42.17	0.90	15.94	4.38	b.d.l.	15.82	16.24	b.d.l.	b.d.l.	0.91	1.03	0.55	97.95
	σ	0.28	0.02	0.18	0.11	–	0.13	0.10	–	–	0.07	0.07	0.04	
1321	29	48.30	1.76	14.81	6.81	0.13	10.09	12.09	1.85	0.15	2.25	0.88	0.47	99.58
	σ	0.67	0.05	0.36	0.12	0.01	0.31	0.30	0.04	0.01	0.02	0.03	0.12	
1322	22	42.91	1.55	13.49	14.75	0.14	9.43	10.58	1.86	0.14	1.94	1.03	0.82	98.63
	σ	0.12	0.03	0.11	0.14	0.02	0.06	0.05	0.04	0.01	0.01	0.01	0.05	
1323	17	37.90	1.38	11.77	24.32	0.14	8.11	9.43	1.64	0.13	1.55	0.73	1.39	98.49
	σ	0.30	0.03	0.16	0.21	0.02	0.25	0.11	0.03	0.01	0.03	0.02	0.09	
1324	16	40.63	1.49	12.72	19.20	0.15	8.70	10.09	1.70	0.14	1.77	0.89	1.03	98.50
	σ	0.88	0.04	0.27	0.48	0.02	0.23	0.27	0.05	0.01	0.01	0.01	0.06	
1325	20	35.19	1.24	11.15	28.62	0.13	8.21	8.65	1.40	0.13	1.50	0.76	1.87	98.84
	σ	0.13	0.02	0.08	0.23	0.02	0.10	0.07	0.02	0.01	0.03	0.01	0.19	
1412	55	53.87	b.d.l.	10.22	0.28	n.m.	12.98	19.71	b.d.l.	n.m.	n.m.	n.m.	4.07	101.13
	σ	0.19	–	0.05	0.04	n.m.	0.07	0.10	–	n.m.	n.m.	n.m.	0.07	
1418	19	46.10	n.m.	10.20	3.79	n.m.	17.44	18.58	n.m.	n.m.	n.m.	n.m.	0.34	96.45
	σ	0.47	n.m.	0.30	0.07	n.m.	0.21	0.10	n.m.	n.m.	n.m.	n.m.	0.02	
1419	26	47.55	n.m.	10.76	3.30	n.m.	17.44	19.77	n.m.	n.m.	n.m.	n.m.	0.34	99.16
	σ	0.28	n.m.	0.12	0.06	n.m.	0.08	0.11	n.m.	n.m.	n.m.	n.m.	0.02	
1425	18	51.78	n.m.	8.88	0.42	n.m.	18.41	15.45	n.m.	n.m.	n.m.	n.m.	6.86	101.80
	σ	0.81	n.m.	0.31	0.07	n.m.	0.17	0.12	n.m.	n.m.	n.m.	n.m.	0.06	
KK38-1	43	51.72	n.m.	13.82	0.54	n.m.	13.51	12.67	n.m.	n.m.	n.m.	n.m.	10.91	103.18
	σ	0.62	n.m.	0.23	0.03	n.m.	0.21	0.17	n.m.	n.m.	n.m.	n.m.	0.12	

Notes: The high totals accompanying high S contents are due to calculation of all cations as oxides. b.d.l = below detection limit. n.m = not measured. Values for Ta and Nb for experiments 1321, 1322, 1323, 1324, and 1325 were obtained by LA-ICP-MS.

TABLE 4. Trace element compositions of silicate and sulfide liquids (ppm)

	Silicates						Sulfides					
Exp. no.	n	Ti	Ce	Nb	Ta	Cu	n	Ti	Ce	Nb	Ta	Cu
390	9	4825	2.7	6111	7428	2.2	8	42	b.d.l.	54	6.1	582
	σ	55	0.1	139	104	0.3	σ	4	–	5	1.5	20
395	9	7268	4.0	8787	11578	3.5	10	45	b.d.l.	52	11	585
	σ	81	0.1	208	186	1.8	σ	6	–	8	4	8
1321	5	10295	204	15704	7182	–	2	77	0.75	95	6.6	–
	σ	31	1	125	210	–	σ	8	0.08	15	0.7	–
1322	5	9248	181	13592	8405	–	5	129	0.92	140	24	–
	σ	48	2	44	56	–	σ	11	0.06	6	2	–
1323	5	7373	144	10842	5946	–	5	226	1.4	272	56	–
	σ	131	2	236	162	–	σ	10	0.3	28	6	–
1324	5	8286	158	12393	7273	–	5	182	1.0	200	37	–
	σ	44	1	73	96	–	σ	11	0.1	9	3	–
1325	5	7138	138	10483	6230	–	6	341	1.7	371	94	–
	σ	75	1	179	112	–	σ	8	0.1	14	3	–
1412	9	522	4.4	8	419	–	9	3266	2.6	4679	3872	–
	σ	23	0.1	2	22	–	σ	434	0.2	618	659	–
1418	7	197	7.5			4.2	6	3.2	0.17			2982
	σ	6	0.1			0.5	σ	1.0	0.08			88
1419	7	186	7.6			2.7	5	3.6	0.13			1885
	σ	15	0.1			0.4	σ	1.4	0.02			66
1425	15	16	4.5			56	11	144	2.4			4743
	σ	4	0.2			3	σ	63	0.2			287
KK38-1	13	b.d.l.	1.7			174	3	182	3.4			10058
	σ	–	0.1			3	σ	21	0.7			1315

TABLE 5. Partition coefficients between sulfide and silicate liquids

Exp. no.	Ti	Ce	Nb	Ta	Cu
390	0.0087	0.0149	0.0089	0.0008	268
σ	0.0008	0.0012	0.0009	0.0002	35
395	0.0062	0.0128	0.0059	0.0010	169
σ	0.0009	0.0052	0.0009	0.0004	87
1321	0.0075	0.0037	0.0061	0.0009	–
σ	0.0007	0.0004	0.0010	0.0001	–
1322	0.014	0.0051	0.010	0.0028	–
σ	0.001	0.0003	0.000	0.0003	–
1323	0.031	0.0095	0.025	0.0094	–
σ	0.001	0.0019	0.003	0.0010	–
1324	0.022	0.0065	0.016	0.0051	–
σ	0.001	0.0005	0.001	0.0004	–
1325	0.048	0.012	0.035	0.015	–
σ	0.001	0.001	0.001	0.001	–
1412	6.3	0.58	604	9.3	–
σ	0.9	0.04	155	1.6	–
1418	0.0164	0.023	–	–	706
σ	0.0049	0.010	–	–	92
1419	0.0196	0.017	–	–	690
σ	0.0078	0.003	–	–	104
1425	8.8	0.53	–	–	84
σ	4.6	0.05	–	–	7
KK38-1	–	2.0	–	–	58
σ	–	0.4	–	–	8

$$\log\gamma_{MS_{n/2}} \cong \log\gamma^{0}_{MS_{n/2}} - \varepsilon^{FeO_{sulf}}_{MS_{n/2}} \log(1 - x^{sulf}_{FeO}) \quad (11)$$

In Equation 11 $\gamma_{MSn/2}$ is the activity coefficient of $MS_{n/2}$ in the sulfide, $\gamma^{0}_{MSn/2}$ is the activity coefficient of $MS_{n/2}$ component at infinite dilution in FeS and $\varepsilon^{FeO_{sulf}}_{MS_{n/2}}$ is the ε-parameter describing interactions between $MS_{n/2}$ and FeO dissolved in the sulfide.

Adding activity coefficients for $MS_{n/2}$ components to Equation 7 gives us a predicted form of $D_M^{sulf/sil}$ of (Kiseeva and Wood 2015):

$$\log D_M^{sulf/sil} \cong A' - \frac{n}{2}\log[FeO] + \varepsilon^{FeO_{sulf}}_{MS_{n/2}} \log(1 - x^{sulf}_{FeO}) \quad (12)$$

In Equation 12, A′ is a constant incorporating end-member properties, [FeO] is, as before the FeO content of the silicate melt and n is the valency of element M.

We assumed valencies of +5 for Nb and Ta, +4 for Ti, and +3

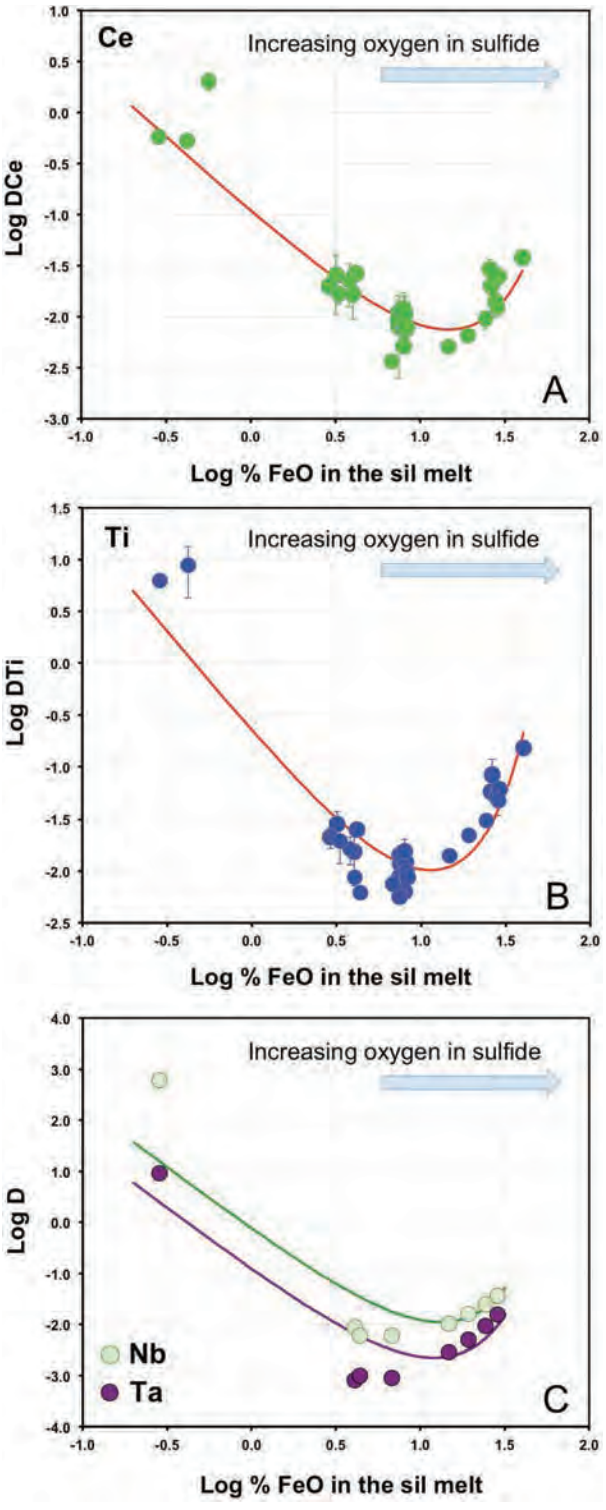

FIGURE 3. Measured partitioning of Ce, Ti, Nb, and Ta between sulfide and silicate at 1.5 GPa and 1400–1460 °C from this study and Kiseeva and Wood (2013, 2015). Curved lines correspond to fits to Equation 12 with assumed oxidation states of +3 for Ce (**a**), +4 for Ti (**b**), and +5 for Nb and Ta (**c**).

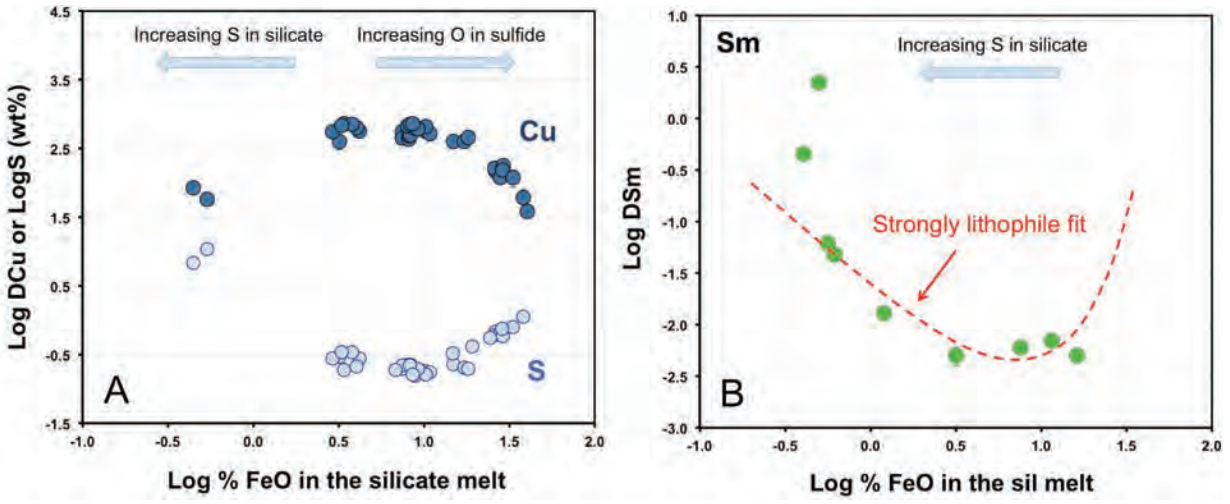

FIGURE 4. (**a**) Partitioning of Cu, $D_{Cu}^{sulf/sil}$ and S concentration at sulfide saturation as functions of the FeO content of the silicate melt. Note that increasing S in the silicate leads to decreasing $D_{Cu}^{sulf/sil}$ at low FeO contents of the silicate. (**b**) Partitioning of Sm $D_{Sm}^{sulf/sil}$ from Wohlers and Wood (2015) plotted in the same manner. The dashed line corresponds to a fit to Equation 12 assuming that Sm has +3 valency. Note the strong deviations from expected behavior at low FeO and high S concentrations in silicate melt.

for Ce to construct fits to the sulfide-silicate partitioning data for these lithophile elements. As can be seen in Figure 3, despite the strongly non-linear behavior, Equation 12 fits the partitioning results extremely well with the addition of the single ε-parameter describing the effects of adding FeO to the sulfide.

At low FeO content the partition coefficient is predicted to converge to the "ideal" slope and this prediction is met reasonably well for Ti^{4+}, Ce^{3+}, and Ta^{5+} (Fig. 3). Note, however, that the likely change of oxidation state of Ti to Ti^{3+} at low FeO content (Mallmann and O'Neill 2009) will tend to "flatten" the slope of logD_{Ti} vs. log[FeO] and hence cause underestimates of D_{Ti} at low [FeO]. A similar phenomenon is observed for Nb because D_{Nb} increases much more steeply than that of the "ideal" slope for Nb^{5+} as log[FeO] is decreased below 0 (Fig. 3c). These observations lead us to consider whether there are additional effects, which apply at very low FeO content of the silicate melt.

LOW FEO ACTIVITY AND ITS EFFECTS ON SULFUR AND TRACE ELEMENT PARTITIONING

In a study of metal-silicate partitioning of trace elements at very low oxygen fugacity it was observed that, at very low FeO contents of the silicate melt, the sulfur partitioning into the silicate increases dramatically (Kilburn and Wood 1997). This observation is consistent with replacement of O (formally O^{2-}) in the silicate melt by S^{2-} in accordance with the equilibrium (O'Neill and Mavrogenes 2002):

$$\underset{\text{sulfide}}{FeS} + \underset{\text{melt}}{O^{2-}} = \underset{\text{melt}}{FeO} + \underset{\text{melt}}{S^{2-}} \quad (13)$$

$$K_{13} = \frac{a_{S^{2-}}.a_{FeO}}{a_{O^{2-}}.a_{FeS}} \quad (14)$$

From the equilibrium constant K_{13} it can readily be seen that, at sulfide saturation (a_{FeS} = 1), lowering the activity of FeO must raise the activity of S^{2-} in the silicate melt and hence the solubility of sulfur in the melt. We tested this hypothesis by adding $FeSi_2$ to our starting mixes to drive the FeO contents of the silicate to very low values.

Figure 4a shows the results of our measurements of S solubility at sulfide saturation as a function of FeO content of the silicate melt. As can be seen (Fig. 4, Table 2) sulfur concentrations in the silicate reach 10.9 wt% as the FeO content declines well below 1 wt%. In such cases the S/(O+S) ratio of the silicate is around 0.1–0.15, which suggests that the sulfur concentration in the silicate may be an important factor in partitioning. It is logical to think that, as the S content of the silicate increases at sulfide saturation the partitioning of chalcophile elements into the sulfide will become less strong as they become more compatible in the S-rich silicate. Similarly, strongly lithophile elements might be expected to be "repelled" by high S contents of the silicate and to partition more strongly than anticipated into coexisting sulfide.

Figure 4a shows partition coefficient $D_{Cu}^{sulf/sil}$ data from this and earlier studies (Kiseeva and Wood 2013, 2015) at 1400–1460 °C and 1.5 GPa. It can clearly be seen that D_{Cu} decreases dramatically, as expected, as the sulfur content of the silicate melt increases in the region of low FeO concentration. Figure 4b shows results for $D_{Sm}^{sulf/sil}$ at 1.5 GPa and 1400–1500 °C (Wohlers and Wood 2015). As suggested above, the pronounced increase in the solubility of sulfur in the silicate as FeO decreases below 1 wt% is accompanied by a dramatic increase in $D_{Sm}^{sulf/sil}$. The effects of increasing S solubility in the silicate are, therefore, the surprising but intuitively reasonable ones of decreasing the partitioning of chalcophile elements and increasing the partitioning of lithophile elements into sulfide relative to silicate.

Discussion and implications

Figures 1, 3, and 4 summarize our current understanding of trace element partitioning between sulfide and silicate melts. Many elements (e.g., Pb, In, Sb, Cd, Co, Zn, Cr) approximate "ideal" behavior, albeit with slopes slightly different from $n/2$ (Fig. 1b). Strongly lithophile elements such as Nb, Ti, and the REE become *chalcophile* at very high and very low FeO contents of the silicate due, respectively, to the increasing oxygen content of the sulfide and the increasing sulfur content of the silicate. The corollary is that chalcophile elements such as Cu, Ag, and Ni become more *lithophile* at both high FeO and low FeO contents of the silicate melt. Thus, one can envision a situation where lithophile Nb partitions more strongly into sulfide than chalcophile Cu because of either the high S content of the silicate or the high oxygen content of the sulfide. Indeed, our data set shows that experiment 1412 with 4 wt% S and 0.28 wt% FeO in the silicate melt has $D_{Nb}^{sulf/sil}$ of 604 while 1425 with 6.9 wt% S and 0.42 wt% FeO has $D_{Cu}^{sulf/sil}$ of 84. Under these, admittedly extreme conditions, Nb is clearly more "chalcophile" than Cu in that it partitions more strongly into sulfide relative to silicate.

Given that nominally lithophile elements can partition strongly into sulfide at low FeO activity, we now consider whether this has any implications for the Earth and other planets. Moderately siderophile (e.g., Ni, Co, Mo, W) and weakly siderophile (e.g., V, Cr, Nb, Si) refractory elements (those that condense at high temperatures from a solar gas) are depleted to varying extents in the bulk silicate Earth relative to lithophile elements of similar volatility (McDonough and Sun 1995). By comparing the Solar System abundances of siderophile with lithophile elements we may calculate the approximate core-mantle partition coefficients of the former (Wade and Wood 2005). These can then be used in conjunction with experimentally determined metal-silicate partition coefficients to construct possible pressure-temperature-oxygen fugacity paths of accretion and core segregation (Wade and Wood 2005). When subsets of the elements of interest are considered it is possible to model core segregation at a single high pressure, temperature, and oxygen fugacity consistent with the current FeO content of bulk silicate Earth. When, however, data for all refractory elements are considered the most consistent solution involves a prolonged period of planetary growth under strongly reducing conditions with low FeO content of the mantle followed by addition of FeO-rich material to bring the oxidized iron content of the mantle up to its current value of 8 wt% (Rubie et al. 2011; Wade and Wood 2005; Wade et al. 2012). Asteroids and planetesimals that may have contributed to an Earth accreting under reducing conditions could have been similar in composition to the enstatite-chondrite meteorites or perhaps to the planet Mercury, which is metal-rich, probably with a S-rich core and has a low FeO, sulfur-rich outer silicate layer (Nittler et al. 2011). In such cases one would anticipate that nominally lithophile elements would be partitioned to some extent between core and mantle, disturbing the expected ratios in the outer silicate part.

The implications of accreting a reduced S-rich body to Earth have been explored in our laboratory by Wohlers and Wood (2015). We found strong partitioning of REE and U into sulfide at low FeO content (Fig. 4b) with the following order of sulfide-silicate partition coefficients for all experiments at 1.5 GPa: $D_U^{sulf/sil} > D_{Nd}^{sulf/sil} > D_{Sm}^{sulf/sil} > D_{Yb}^{sulf/sil}$ (Wohlers and Wood 2015). In general, $D_{Nd}^{sulf/sil} \approx 1.4 D_{Sm}^{sulf/sil}$ and $D_{Th}^{sulf/sil} \approx 0.1 D_U^{sulf/sill}$. The implications are that, in a reduced S-rich body such as Mercury, addition of sulfide to the core would carry U with it together with strong fractionation of Nd relative to Sm. Addition of a similar body to Earth during accretion could provide significant energy in the form of U and Th added to the core to drive the geodynamo (Wohlers and Wood 2015). Furthermore, the silicate part of such a body would have superchondritic Sm/Nd with, as observed (Boyet and Carlson 2005) a positive ^{142}Nd anomaly relative to chondritic meteorites. It appears, therefore, that addition of reduced, S-rich bodies to the accreting Earth provide a possible explanation both for slow cooling of the core and for the non-chondritic Sm/Nd ratio of the silicate Earth.

Given our observations and considering the ubiquitous nature of both quenched sulfide melts and solid sulfides in igneous rocks it is clear that there is much more to be discovered about the geochemical behavior of sulfides in igneous petrogenesis. As yet, we have only scratched the surface.

Acknowledgments

We acknowledge support from the European Research Council, grant 267764 to B.J.W. and the NERC grant NE/L010828/1 to E.S.K. We thank Youxue Zhang and Neil Bennett for their comments and for their help in improving the manuscript.

References cited

Boyet, M., and Carlson, R.W. (2005) ^{142}Nd evidence for early (>4.53Ga) global differentiation of the silicate Earth. Science, 309, 576–581.

Dreibus, G., and Palme, H. (1996) Cosmochemical constraints on the sulfur content in the Earth's core. Geochimica et Cosmochimica Acta, 60, 1125–1130.

Falloon, T.J., and Green, D.H. (1987) Anhydrous partial melting of MORB pyrolite and other peridotite compositions at 10kb: Implications for the origin of primitive MORB glasses. Contributions to Mineralogy and Petrology, 37, 181–219.

Hart, S.R., and Gaetani, G.A. (2006) Mantle Pb paradoxes: The sulfide solution. Contributions to Mineralogy and Petrology, 152, 295–308.

Hofmann, A.W., Jochum, K.P., Seufert, M., and White, W.M. (1986) Nb and Pb in Oceanic Basalts—New Constraints on Mantle Evolution. Earth and Planetary Science Letters, 79, 33–45.

Kilburn, M.R., and Wood, B.J. (1997) Metal-silicate partitioning and the incompatibility of S and Si during core formation. Earth and Planetary Science Letters, 152, 139–148.

Kiseeva, E.S., and Wood, B.J. (2013) A simple model for chalcophile element partitioning between sulphide and silicate liquids with geochemical applications. Earth and Planetary Science Letters, 383, 68–81.

——— (2015) The effects of composition and temperature on chalcophile and lithophile element partitioning into magmatic sulphides. Earth and Planetary Science Letters, 424, 280–294.

Lee, C.T.A., Luffi, P., Chin, E.J., Bouchet, R., Dasgupta, R., Morton, D.M., Le Roux, V., Yin, Q.Z., and Jin, D. (2012) Copper systematics in arc magmas and implications for crust-mantle differentiation. Science, 336, 64–68.

Ma, Z.T. (2001) Thermodynamic description for concentrated metallic solutions using interaction parameters. Metallurgical and Materials Transactions B, 32, 87–103.

Mallmann, G., and O'Neill, H.St.C. (2009) The crystal/melt partitioning of V during mantle melting as a function of oxygen fugacity compared with some other elements (Al, P, Ca, Sc, Ti, Cr, Fe, Ga, Y, Zr and Nb). Journal of Petrology, 50, 1765–1794.

McDade, P., Wood, B.J., Van Westrenen, W., Brooker, R., Gudmundsson, G., Soulard, H., Najorka, J., and Blundy, J. (2002) Pressure corrections for a selection of piston-cylinder cell assemblies. Mineralogical Magazine, 66, 1021–1028.

McDonough, W.F., and Sun, S.-s. (1995) The composition of the Earth. Chemical Geology, 120, 223–253.

Nittler, L.R., Starr, R.D., Weider, S.Z., McCoy, T.J., Boynton, W.V., Ebel, D.S., Ernst, C.M., Evans, L.G., Goldsten, J.O., Hamara, D.K., and others. (2011) The major-element composition of Mercury's surface from MESSENGER

X-ray spectrometry. Science, 333, 1847–1850.
O'Neill, H.St.C. (1991) The origin of the Moon and the early history of the Earth—A chemical model 2. The Earth. Geochimica et Cosmochimica Acta, 55, 1159–1172.
O'Neill, H.St.C., and Mavrogenes, J.A. (2002) The sulfide capacity and the sulfur content at sulfide saturation of silicate melts at 1400°C and 1 bar. Journal of Petrology, 43, 1049–1087.
Presnall, D.C., Dixon, S.A., Dixon, J.R., O'Donnell, T.H., Brenner, N.L., Schrock, R.L., and Dycus, D.W. (1978) Liquidus phase relations on the join diopside-forsterite-anorthite from 1atm to 20kbar: Their bearing on the generatin and crystallization of basaltic magma. Contributions to Mineralogy and Petrology, 66, 203–220.
Rubie, D.C., Frost, D.J., Mann, U., Asahara, Y., Nimmo, F., Tsuno, K., Kegler, P., Holzheid, A., and Palme, H. (2011) Heterogeneous accretion, composition and core-mantle differentiation of the Earth. Earth and Planetary Science Letters, 301, 31–42.
Wade, J., and Wood, B.J. (2005) Core formation and the oxidation state of the Earth. Earth and Planetary Science Letters, 236, 78–95.
Wade, J., Wood, B.J., and Tuff, J. (2012) Metal-silicate partitioning of Mo and W at high pressures and temperatures: Evidence for late accretion of sulphur to the Earth. Geochimica et Cosmochimica Acta, 85, 58–74.
Wagner, C. (1962) Thermodynamics of Alloys. Addison-Wesley, Reading, Massachusetts.
Wohlers, A., and Wood, B.J. (2015) A Mercury-like component of early Earth yields uranium in the core and high mantle Nd-142. Nature, 520, 337–340.
Wood, B.J., and Halliday, A.N. (2005) Cooling of the earth and core formation after the giant impact. Nature, 437, 1345–1348.

Manuscript received March 20, 2015
Manuscript accepted June 1, 2015
Manuscript handled by David London